



1 **Spatiotemporal ITCZ dynamics during the last three millennia in**
2 **Northeastern Brazil and related impacts in modern human history**

3

4 Giselle Utida^{1*}, Francisco W. Cruz¹, Mathias Vuille², Angela Ampuero¹, Valdir F. Novello³,
5 Jelena Maksic⁴, Gilvan Sampaio⁵, Hai Cheng^{6,7,8}, Haiwei Zhang⁶; Fabio Ramos Dias de
6 Andrade¹, R. Lawrence Edwards⁹

7

8 ¹Instituto de Geociências, Universidade de São Paulo, Rua do Lago, 562, Cidade Universitária,
9 São Paulo-SP, 05508-090, Brazil

10 ²Department of Atmospheric and Environmental Sciences, University at Albany, SUNY, Albany, NY,
11 USA

12 ³Geo- and Environmental Research Center, University of Tübingen, Tübingen, Germany

13 ⁴Division of Impacts, Adaptation and Vulnerabilities (DIIAV), National Institute for Space Research
14 (INPE), São Jose dos Campos-SP, Brazil

15 ⁵General Coordination of Earth Science (CGCT), National Institute for Space Research (INPE), Sao
16 Jose dos Campos-SP, Brazil

17 ⁶Institute of Global Environmental Change, Xi'an Jiaotong University, Xi'an, China

18 ⁷State Key Laboratory of Loess and Quaternary Geology, Institute of Earth Environment, Chinese
19 Academy of Sciences, Xi'an, China

20 ⁸Key Laboratory of Karst Dynamics, MLR, Institute of Karst Geology, CAGS, China

21 ⁹Department of Earth Sciences, University of Minnesota, Minneapolis, MN, USA

22 *Corresponding author: giselleutida@hotmail.com

23

24

25

26

27



28 *Abstract*

29 Changes in tropical precipitation over the past millennia have usually been associated with
30 latitudinal displacements of the Intertropical Convergence Zone (ITCZ). Recent studies
31 provide new evidence that contraction and expansion of the tropical rainbelt may also have
32 contributed to ITCZ variability on centennial time scales. Over tropical South America few
33 records point to a similar interpretation, which prevents a clear diagnosis of ITCZ changes
34 in the region. In order to improve our understanding of the equatorial rainbelt variability, our
35 study presents a reconstruction of precipitation for the last 3200 years from the Northeast
36 Brazil (NEB) region, an area solely influenced by ITCZ precipitation. We analyze oxygen
37 isotopes in speleothems that serve as a faithful proxy for the past location of the southern
38 margin of the ITCZ. Our results, in comparison with other ITCZ proxies, indicate that the
39 range of seasonal migration, contraction and expansion of the ITCZ was not symmetrical
40 around the equator. A new NEB ITCZ pattern emerged based on the comparison between
41 two distinct proxies that characterize the ITCZ behavior during the last 2500 years, with an
42 ITCZ zonal pattern between NEB and the eastern Amazon. In NEB, the period related to the
43 Medieval Climate Anomaly (MCA) was characterized by an abrupt transition from wet to dry
44 conditions. These drier conditions persisted until the onset of the period corresponding to
45 the Little Ice Age (LIA), representing the longest dry period over the last 3200 years in NEB.
46 The ITCZ was apparently forced by teleconnections between Atlantic Multidecadal
47 Variability and Pacific Decadal Variability that controlled the position, intensity and width of
48 Walker cell over South America changing the ITCZ zonally, and sea surface temperature
49 changes in both the Pacific and Atlantic, stretching/weakening the ITCZ-related rainfall
50 meridionally over NEB. Wetter conditions started around 1500 CE in NEB. During the last
51 500 years, our speleothems document the occurrence of some of the strongest drought
52 events for the last millennia, which drastically affected population and environment of NEB



53 during the Portuguese colonial period. The historical droughts were able to affect the karst
54 system, and led to significant impacts over the entire NEB region.

55

56 *Keywords:* Holocene, speleothems, stable isotopes, droughts, Portuguese colony

57

58 1. Introduction

59

60 Northeastern Brazil (NEB) is one of the areas in South America (SA) most vulnerable
61 to the impacts of climate change. The semi-arid conditions in NEB are strongly affected by
62 precipitation variability, and since the 18th century the region has experienced more frequent
63 drought events. Today the frequent droughts put ~57 million people, ~27% of the Brazilian
64 population, at risk of experiencing water scarcity (Marengo and Bernasconi, 2015; Lima and
65 Magalhães, 2018). Aside from native people, the region has been occupied since the
66 Portuguese colonization in the 16th century, and the ensuing intense agricultural activity has
67 been responsible for a large-scale degradation of the Caatinga biome, the typical vegetation
68 of NEB's semi-arid areas. This land mismanagement and the increasing frequency of
69 regional droughts has put some of these areas at great risk of desertification (Marengo and
70 Bernasconi, 2015; Sampaio et al., 2020). Advancing our knowledge about NEB's climate
71 and recurrence of extreme events in a long-term context is therefore of great importance to
72 better anticipate the impacts of these intense and abrupt drought events.

73 The Intertropical Convergence Zone (ITCZ) is one of the key elements responsible
74 for precipitation over NEB, which is also indirectly affected by the South American Summer
75 Monsoon (SASM). When the ITCZ is in its southernmost position during austral autumn,
76 northern areas of NEB experience increased precipitation (Schneider et al., 2014), while the
77 precipitation in the southern areas of NEB occurs mainly during austral summer in response
78 to climatic conditions in the tropical South Atlantic (Vera et al., 2006; Vuille et al., 2012).



79 Although these systems are independent and arise in different seasons, the position of the
80 ITCZ affects SASM intensity and its development through moisture influx to the continent
81 (Vuille et al., 2012; Schneider et al., 2014).

82 On orbital to centennial timescales, weakened precipitation in NEB has been
83 associated with enhanced subsidence over NEB during intense SASM periods (Cruz et al.,
84 2009; Orrison et al., 2022), giving rise to a zonal dipole between the western Amazon and
85 NEB (Cruz et al., 2009; Novello et al., 2018). This mode also operates today on interannual
86 and seasonal time scales (Lenters and Cook, 1997; Sulca et al., 2016).

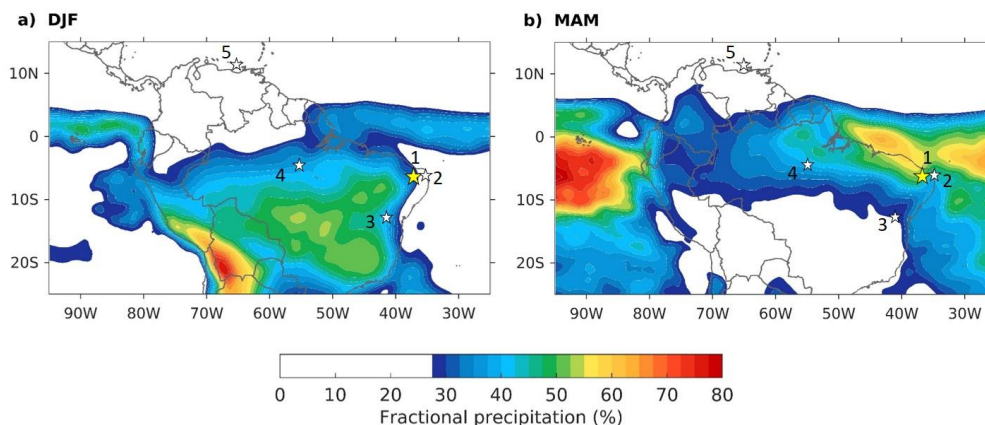
87 More recent studies suggested that these variations on millennial and centennial
88 timescales in NEB may also have been caused by contraction or expansion of the ITCZ
89 affecting the precipitation over South America (Utida et al., 2019; Chiessi et al., 2021). These
90 ITCZ dynamics would be forced by changes in tropical Atlantic and Pacific SST and related
91 atmospheric circulation changes (e.g., Lechleitner et al., 2019; Utida et al., 2019; Chiessi et
92 al., 2021; Steinman et al., 2022). These results suggest complex ITCZ dynamics operating
93 over NEB; a region where the lack of studies complicates the paleoclimate interpretations
94 for the last millennia.

95 In comparison with the ITCZ, the SASM has received more attention from recent
96 studies, mainly due to its larger area of influence in SA, extending from the tropical Andes
97 to the Amazon and southeastern SA (e.g., Apaéstegui et al., 2018; Azevedo et al., 2019;
98 Della Libera et al., 2022). The spatiotemporal precipitation variability over tropical SA during
99 the Common Era (CE) was evaluated based on a network of high-resolution proxy records
100 (Novello et al., 2018; Campos et al., 2019; Orrison et al., 2022). These studies point to an
101 association between SASM variability and the latitudinal displacement of the ITCZ, although
102 changes in the latitude of the ITCZ during the last millennia are not well established.

103 Previous studies based on oxygen and hydrogen isotopes from paleorecords
104 obtained in NEB have served as useful proxies for ITCZ precipitation in the region (Cruz et



105 al., 2009; Utida et al., 2019, 2020), while carbon isotopes have been used to interpret soil
106 erosion/production and vegetation cover (Utida et al., 2020; Novello et al., 2021; Azevedo
107 et al., 2021). Building on these recent advances, we present an ITCZ precipitation
108 reconstruction based on stalagmite records from the state of Rio Grande do Norte (RN),
109 located at the modern southernmost limit of the ITCZ in eastern South America (Fig 1). By
110 using oxygen and carbon isotopes obtained from these stalagmites, we reconstruct
111 precipitation and vegetation/soil cover over the last 3,200 years over NEB. These data are
112 essential to fill the gap of high-resolution records in NEB and to improve the interpretation
113 of ITCZ dynamics over SA and how they are related to SASM variability during the CE.



114

115 Figure 1 – Location and precipitation climatology of study sites during the austral
116 summer (DJF - December to February) and autumn (MAM - March to May). Color shading
117 of regions above 27.5% of annual precipitation highlights the extent of the (a) SASM over
118 the continent and (b) the ITCZ over the ocean. Precipitation data from the Global
119 Precipitation Measurement (GPM) mission, with averages calculated over period 2001–
120 2020. 1) Trapiá and Furna Nova Cave (yellow star, this study), 2) Boqueirão Lake (Utida et
121 al., 2019), 3) Diva de Maura Cave (Novello et al., 2012), 4) Paraíso Cave (Wang et al.,
122 2017), 5) Cariaco Basin (Haug et al., 2001).



123 *2. Regional settings*

124

125 *2.1. Study area*

126 We study stalagmites from two caves located in the Rio Grande do Norte State, in
127 northern NEB (Fig 1), Trapiá and Furna Nova Cave. The caves were developed in the
128 Cretaceous carbonate rocks of the Jandaíra Formation, Potiguar Basin, close to the Apodi
129 River valley (Pessoa-Neto, 2003; Melo et al., 2016). The exposed karst pavements extend
130 over several kilometers and include a series of small canyon-like caves that usually are no
131 more than 40 m deep (Silva et al., 2017). We collected speleothems in Trapiá and Furna
132 Nova caves. Trapiá Cave (5°33'45.43"S, 37°37'15.92"W) is a 2330 m long cave with 29 m
133 of bedrock above the cave cavity. This cave is located 90 km from the Atlantic coast and ~
134 50 m above sea level, with temperature and relative humidity at the chamber of 28.5°C and
135 100%, respectively. Furna Nova Cave (5°2'3.22"S, 37°34'16"W) is located 60 km north of
136 Trapiá Cave, 45 km from the Atlantic coast and ~95 m above sea level. The cave is 239.3
137 m long, with 29.8 m of bedrock above the cave cavity. Its temperature and relative humidity
138 at the speleothem chamber are 25°C and 95.0%, respectively.

139 The annual mean temperature is around 28°C (INMET - National Institute of
140 Meteorology – Instituto Nacional de Meteorologia – data from 1961-1990) and average
141 precipitation is approximately 730 mm/year, concentrated in the period between March and
142 May, during the southernmost position of the ITCZ (Agência Nacional de Águas – ANA -
143 National Agency of Waters, 2013; Ziese et al., 2018). Caatinga dry forest is the typical
144 vegetation of the region. It is adapted to short rainy seasons of 3 to 4 months in length and
145 tolerates large interannual variations in precipitation. It is characterized by sparse dry forest,
146 dominated by arboreal deciduous shrubland (Erasmí et al., 2009).

147

148 *2.2. Climatology*



149 The drylands of NEB extend from 2.5°S to 16.1°S, and from 34.8°W to 46°W, with
150 an area of about 1,542,000 km², representing 18.26% of Brazilian territory (Marengo and
151 Bernasconi, 2015). Although the whole area is classified as semi-arid and has faced intense
152 droughts, especially influenced by El Niño, there are significant differences in climatic
153 systems between the northern and southern sectors of NEB. Furthermore, the NEB eastern
154 coastal sector is characterized by a different rainfall seasonality, receiving more rainfall
155 across the year, as the climate in this region is modulated by the sea breeze circulation and
156 easterly wave disturbances during June and July (Gomes et al., 2015; Marengo and
157 Bernasconi, 2015; Utida et al., 2019).

158 Northern NEB (N-NEB), where the studied caves are located, receives most of its
159 precipitation from March to May, when the seasonal migration of the ITCZ reaches its
160 southernmost position (Fig 2a) (Schneider et al., 2014; Utida et al., 2020), and ITCZ-related
161 precipitation extends across the equator southward to NEB (Fig 1).

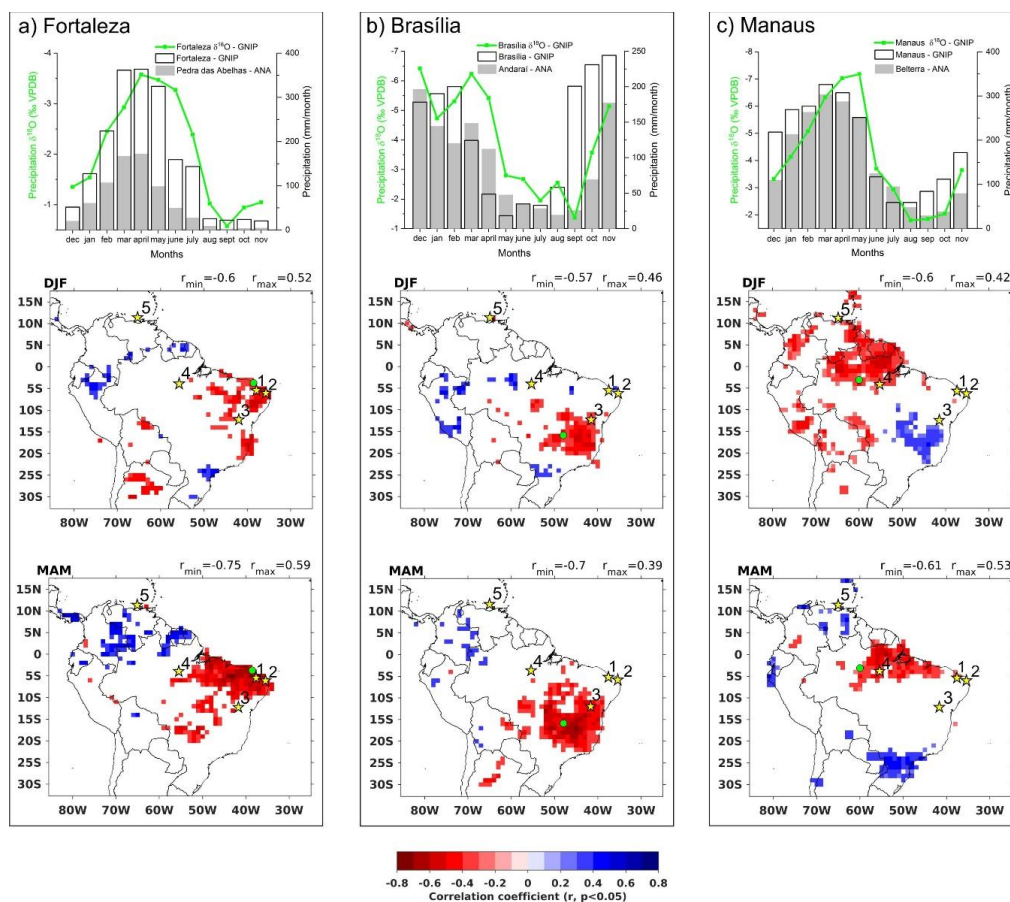
162 In N-NEB, we analyzed precipitation data of Pedra das Abelhas Station – RN (Fig
163 2a), from 1911 to 2015 (n=103). In order to exclude possible extreme events with a known
164 forcing, we excluded the most significant years of El Niño - Southern Oscillation (ENSO) (39
165 years), according to Araújo et al. (2013). The results (Fig S1) reveal that in the majority of
166 years (interquartile range) the total rainy season persists from February to April, with
167 precipitation varying from 100 to 180 mm/month, and minor contributions occurring in
168 January and May (50-70 mm/month). During the driest years (25% of quantiles), the rainy
169 season persists also from February to April, but the maximum precipitation is below 90
170 mm/month, while during the wettest years (75% of quantiles), the rainy season starts in
171 January with more than 100 mm/month and lasts until May with almost 150 mm/month,
172 reaching values higher than 250 mm around March. These data show that years with
173 increased precipitation amounts are characterized by a longer rainy season, while the
174 precipitation deficit during drought years is primarily the result of a shorter rainy season. The



175 anomalous length of the rainy season can be attributed to variations in the meridional SST
176 gradient in the tropical Atlantic that result in a shift of the ITCZ to the north or south of its
177 climatological position (e.g., Andreoli et al., 2011; Marengo and Bernasconi, 2015; Alvalá et
178 al., 2019).

179 In S-NEB, the precipitation occurs mainly during summer, from December to
180 February (Fig 1a and 2b). This regional seasonality difference with N-NEB is evident in the
181 spatial correlation map between GPCP precipitation anomalies (Schneider et al., 2011) and
182 $\delta^{18}\text{O}$ anomalies obtained from IAEA-GNIP (International Atomic Energy Agency - Global
183 Network of Isotopes in Precipitation) for Fortaleza and Brasília (the closest IAEA station to
184 Diva de Maura Cave) stations. The reddish areas on the map indicate significant negative
185 correlations during the austral summer (DJF) and autumn (MAM) between the local
186 precipitation $\delta^{18}\text{O}$ signals and the regional precipitation amount. Overall, the spatial
187 correlations indicate that in both areas the amount effect is the dominant effect on the
188 isotopic composition of rainfall (Dansgaard, 1964). However, the isotopic signal varies
189 seasonally and as a function of the two different circulation systems. The negative spatial
190 correlation observed over N-NEB suggests precipitation is dominated by ITCZ dynamics,
191 similar to the conditions over Fortaleza, while the negative spatial correlation over S-NEB
192 (Fig 2b) is a result of the rainfall influenced by the SASM (Fig 1) (Vera et al., 2006), such as
193 in Brasília city, in central Brazil. Therefore, precipitation and the associated isotopic signal
194 are the result of ITCZ dynamics in N-NEB, while they are influenced by the SASM in the S-
195 NEB. Accordingly, their rainfall seasonality is also different (Fig 2), with a NDJFM peak in
196 the south (Brasília) and a MAM rainfall peak in the north (Fortaleza).

197



198

199

200

201

202

203

204

205

206

207

208

Figure 2 – NEB correlation map between regional precipitation amount and oxygen isotope ratios for GNIP stations (IAEA-WMO, 2021) (green dots) and precipitation amount for ANA stations: (a) Fortaleza GNIP station and precipitation at Pedra das Abelhas station in northern NEB, (b) Brasília GNIP station and precipitation at Andaraí station (star 3) in southern NEB, c) Manaus GNIP station and precipitation at Belterra station (star 4) in the eastern Amazon. The maps show the spatial correlation between $\delta^{18}\text{O}$ anomalies at GNIP stations and GPCP gridded precipitation anomalies for December to February (DJF) and March to May (MAM) for Fortaleza, Brasília and Manaus GNIP stations (Ziese et al., 2018). The $\delta^{18}\text{O}$ values and precipitation for each station were obtained from GNIP IAEA/WMO database. The reference period for analysis is 1960-2016. Stars indicate the site locations:



209 1) Trapiá Cave, Furna Nova Cave and Pedra das Abelhas ANA Station, 2) Boqueirão Lake
210 (Utida et al., 2019), 3) Diva de Maura Cave (Novello et al., 2012) and Andaraí ANA Station,
211 4) Paraíso Cave (Wang et al., 2017) and Belterra ANA Station, 5) Cariaco Basin (Haug et
212 al., 2001).

213

214 Another important region in SA affected by the ITCZ behavior is the eastern Amazon,
215 west of the NEB, where the Paraiso speleothem isotope record was retrieved (Fig 1 and Fig
216 2). This region is characterized by increased precipitation during DJFMAM and a peak in
217 rainfall and a $\delta^{18}\text{O}$ minimum in MAM (Fig 2c) as a result of precipitation received from the
218 ITCZ in both summer and autumn. It can be depicted by the negative correlation between
219 $\delta^{18}\text{O}$ at the Manaus GNIP station and rainfall over the upstream equatorial region under
220 direct ITCZ influence. In addition, there is only a minor influence through water recycling
221 over the Amazon Basin, due to its proximity to the coast (Wang et al., 2017).

222

223 3. Materials and Methods

224

225 Four stalagmites were collected in northern NEB caves, two at Trapiá Cave, TRA5
226 and TRA7 that are 178 and 270 mm long, respectively (Fig S2), and two at Furna Nova, FN1
227 and FN2 with a length of 202 and 95 mm, respectively (Fig S3). The stalagmite FN1 was
228 previously studied by Cruz et al. (2009) for chronology and oxygen isotopes. Utida et al.
229 (2020) also studied TRA7 for chronology and carbon isotopes. These samples are part of
230 the speleothem collection of the Geoscience Institute at the University of São Paulo.

231 Chronological studies on speleothems were based on U-Th geochronology
232 performed at the Laboratories of the Department of Earth and Environmental Sciences,
233 College of Science and Engineering, University of Minnesota (USA), and at the Institute of
234 Global Environmental Change, Xi'an Jiaotong, University of Xi'an (China), using an



235 inductively coupled plasma-mass spectrometry (MC-ICP-MS Thermo-Finnigan NEPTUNE)
236 technique, according to Cheng et al. (2013). Age models of speleothem TRA5 and FN2 were
237 based on 12 and 10 uranium U/Th dates, respectively (Table S1 and S2). The FN1
238 chronology is based on 10 previously published U/Th results obtained by Cruz et al. (2009)
239 plus 8 additional new dates obtained for this study (Table S1). Speleothem TRA7 has 27
240 U/Th ages that were presented in Utida et al. (2020). The individual age models for all
241 speleothems were constructed by the software COPRA (Breitenbach et al., 2012) through a
242 set of 2,000 Monte Carlo simulations, where a random age within the $\pm 1\sigma$ age interval was
243 chosen each time.

244 For oxygen and carbon isotope analysis of the speleothems, around 200 μg of
245 powder was drilled for each sample, consecutively at intervals of 0.1 mm (TRA5), 0.3 mm
246 (TRA7) and 0.15 mm (FN2), with a Micromill micro-sampling device. These samples were
247 prepared using an online automated carbonate preparation system and analyzed by a
248 GasBench interfaced to a Thermo Finnigan Delta V Advantage at the Laboratory of Stable
249 Isotopes (LES) at the Geoscience Institute of the University of São Paulo. Isotopes are
250 reported in delta notation ($\delta^{18}\text{O}$ and $\delta^{13}\text{C}$) relative to the Vienna Pee Dee Belemnite (VPDB)
251 standard, with uncertainties in the reproducibility of standard materials $< 0.1\%$. The isotopic
252 profiles of TRA5, TRA7, FN1 and FN2 stalagmites consist of 443, 885, 1215 and 651 isotope
253 samples, respectively. These datasets provide an average resolution of ~ 1 year per sample
254 for TRA5 and ~ 4 years for the other speleothem records. TRA7 $\delta^{13}\text{C}$ results were presented
255 by Utida et al. (2020) and FN1 $\delta^{18}\text{O}$ results by Cruz et al. (2009) using the same methods.
256 Cruz et al. (2009) do not provide FN1 $\delta^{13}\text{C}$ results, which were not included in this study.

257 Different textural characteristics of speleothem TRA5 and FN2 were identified in
258 intervals which were analyzed for mineralogical composition based on approximately 20 mg
259 samples with X-ray powder diffraction in a Bruker D8 diffractometer (Cu Ka, 40 kV, 40 mA,



260 step 0.02°, 153 s/step, scanning from 3 to 105° 2 θ) at the NAP Geoanalítica Laboratory of
261 the University of São Paulo. Qualitative and quantitative mineralogical analyses were
262 performed with *Match!* and *FullProf* software, using the Crystallographic Open Database
263 (Grazulis et al., 2009). Crystallographic data for the mineral phases were taken from Pokroy
264 et al. (1989) for aragonite and from Paquette and Reeder (1990) for calcite. Mineralogical
265 results of TRA7 and FN1 were obtained by Utida et al. (2020) using the same method. All
266 results are presented in weight proportion (wt %). The $\delta^{18}\text{O}$ results of speleothems were
267 calibrated according to the percentage of calcite identified for the interval applying the
268 aragonite–calcite fractionation offset of $0.85\text{‰} \pm 0.29\text{‰}$ (Zhang et al., 2014). The $\delta^{13}\text{C}$
269 results were not corrected because the original aragonite–secondary calcite fractionation
270 factor is negligible ($-0.1\text{--}0.2\text{‰}$) (Zhang et al., 2014). Even considering the original aragonite–
271 original calcite mean fractionation factor of 1.1‰ (Zhang et al., 2015), the range of $\delta^{13}\text{C}$ RN
272 stalagmites is very large ($>8\text{‰}$) and the correction would not affected the main interpretation.

273 The intra-site correlation model (*iscam*) was used to construct a composite record
274 (Fohlmeister, 2012). It combined the climate records to obtain a unique age model and
275 oxygen isotopic record, corrected only for mineralogical composition for speleothems from
276 Rio Grande do Norte, which here is referred to as the RN Composite. The age-depth
277 modeling software was adjusted to calculate 1000 Monte-Carlo simulations on absolute age
278 determinations to find the best correlation between oxygen isotope records from Trapiá and
279 Furna Nova speleothems, reproducing adjacent archives. The results estimate the error of
280 the age-depth model by indicating the 68%, 95% and 99% confidence intervals obtained
281 from evaluation of a set of 2000 first order autoregressive processes (AR1) for each record.
282 This method allows significantly reducing the age uncertainty within the overlapping periods
283 and it can be tested if the signal of interest is indeed similar in all the records (Fohlmeister,
284 2012). The age data were assumed to have a Gaussian distribution and were calculated



285 pointwise. The composite result was detrended and normalized, according to the *iscam*
286 method. The performance of the *iscam* results is affected by low quality of chronological
287 control, low resolution and hiatuses. Therefore, the following intervals were removed from
288 the stalagmite records before constructing the RN Composite: FN1 0-12 mm and 187-202
289 mm, FN2 0-6 mm, TRA5 0-37mm and TRA7 222-227 mm. In addition, the FN1 record was
290 divided into two portions: FN1a 12.14-136.99 mm and FN1b 140.15-186.87 mm that are
291 separated by a hiatus. The chronological age-depth relationship in the overlapping parts of
292 the individual stalagmites was modified and improved according to the *iscam* results of the
293 composite record.

294

295 4. Results

296

297 4.1. Chronology and mineralogy

298 The RN record covers the last 5000 years, four stalagmites cover the last 3250 years,
299 and two of these stalagmites cover partially between 3000 and 1260 Before Common Era
300 (BCE), with the exception of one hiatus at 2100 -1720 years BCE (Fig 3, Table S1 and S2).

301 Stalagmite TRA7 from Trapiá Cave was deposited from 3000 to 2180 BCE (Fig S4)
302 with a low deposition rate (DR) of approximately 0.05 mm/yr. After a hiatus of 1880 years, it
303 resumed deposition from at 300 BCE until 1940 CE with a DR of 0.18 mm/yr. The TRA5
304 stalagmite deposition occurred continuously from 1490 to 1906 CE (Fig S4) with a DR of
305 0.33 mm/yr.

306 Stalagmite FN1 from Furna Nova was deposited over the last 3,600 years, with a
307 hiatus from 125 to 345 BCE and another one of approximately 100 years between 1525 and
308 1662 CE (Fig S4), with an average DR of 0.09 mm/yr. The FN2 stalagmite deposited
309 continuously from 1226 BCE to 7 CE, except for a hiatus between 189 and 45 BCE (Fig S4)
310 with a DR of 0.20 mm/yr.



311 The mineralogy of the stalagmites from Trapiá Cave is formed by layers of crystals
312 with mosaic and columnar fabrics, composed exclusively of calcite, except for the base
313 portion of TRA7 from 173 to 270 mm (3,000 BCE to 130 CE), which is described as an
314 interbedded needle-like crystals texture, composed of 87.1 to 99% of aragonite (Fig S2,
315 Table S3). The same needle-like morphology is present in most of the Furna Nova Cave
316 stalagmites, composed of aragonite with a weight proportion greater than 85% in FN1,
317 extending from 0 to 83 mm (160 to 1,340 CE) and from 128 to 183 mm (1,730 BCE to 80
318 CE). In the FN2 sample this weight proportion is greater than 93.4% (1265 BCE to 35 CE).
319 The only interval composed of 100% calcite is from 95 to 125 mm in FN1 (Fig S3, Table S3).
320 These speleothem samples show no sign of dissolution or recrystallization.

321

322 4.2. Stalagmite $\delta^{18}\text{O}$ and $\delta^{13}\text{C}$

323 The oxygen isotope ratios of the RN record vary from 0.6‰ to -4.5‰, with mean
324 values for each speleothem of -2.8‰ for TRA7, -3.5‰ for TRA5, -2.4‰ for FN1 and -1.5‰
325 for FN2. Similarities among the stalagmites are evident, especially around 1500 CE when
326 $\delta^{18}\text{O}$ values abruptly decrease in TRA7 and TRA5, while in FN2 this period features a hiatus.

327 These values were slightly changed by the correction for aragonite–calcite
328 fractionation ($\delta^{18}\text{O}_{\text{C-A}}$) (Zhang et al., 2014), according to their aragonite weight proportion
329 (Table S3, Fig 3b). The isotopic correction due to mineralogy for the stalagmites from Furna
330 Nova Cave resulted in changes of less than 0.1‰ of their mean values. The mean correction
331 for TRA7 equals an enrichment of 0.5‰ during the first 1800 years. Values from TRA5 were
332 corrected along the entire sample by adding 0.85‰, as it is composed of 100% calcite.
333 Therefore, the mean values increased from -3.5‰ to -2.7‰.

334 Four main phases describe the $\delta^{13}\text{C}$ dataset (Fig 3a). The oldest phase from 3000
335 to 2160 BCE is characterized by $\delta^{13}\text{C}$ values close to zero. After a hiatus (2170-1270 BCE)



336 there is a short interval of stability with $\delta^{13}\text{C}$ values around -4‰ that lasts from 1270 to 840
337 BCE and is followed by a $\delta^{13}\text{C}$ enrichment that reaches a value of zero at 30 CE. Between
338 30 and 1500 CE there is a trend toward more negative $\delta^{13}\text{C}$ values, varying from 0 to -8.8‰ .
339 This interval is marked by a valley at 190 CE with $\delta^{13}\text{C}$ values of -7.2‰ and a peak at 1000
340 CE with $\delta^{13}\text{C}$ values of 0.22‰ . The youngest period, from 1500 to 1930 CE is more stable
341 than the previous one, with $\delta^{13}\text{C}$ values averaging around -6.4‰ .

342

343 *4.3. Composite*

344 Combining the $\delta^{18}\text{O}$ results from the four RN stalagmites allows establishing a
345 continuous record covering the last ~ 3200 years, the RN Composite (Fig 4). The correlation
346 coefficient (r) between each measured $\delta^{18}\text{O}$ stalagmite time series is >0.59 , significant at
347 the 95% level (Fig S5). The composite provides an average temporal resolution of ~ 2 years.
348 The entire stable isotope time series is composed of 2495 $\delta^{18}\text{O}$ measurements, corrected
349 according to mineralogical composition.

350

351 *5. Discussion*

352

353 *5.1. Paleoclimate interpretation*

354

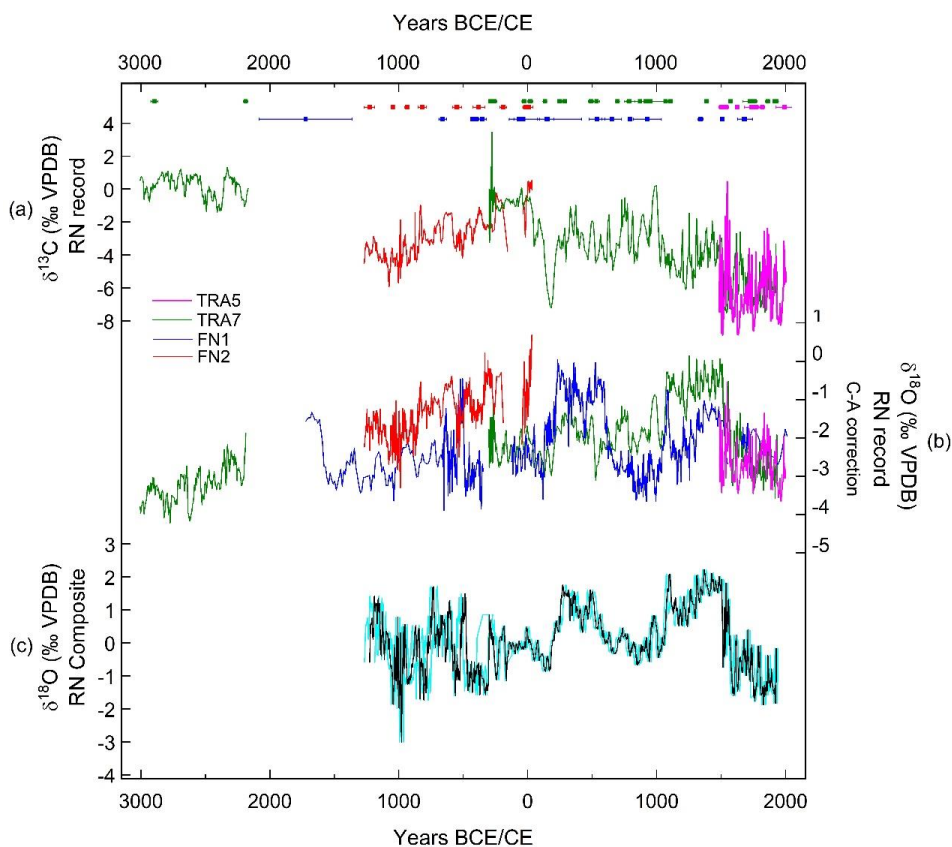
355 The $\delta^{18}\text{O}$ RN Composite allowed us to reconstruct precipitation changes influenced
356 by the ITCZ position in N-NEB and its convective intensity. This interpretation is based on
357 the spatial correlation between $\delta^{18}\text{O}$ at GNIP stations and GPCC precipitation (Fig 2).
358 Highest precipitation amounts occur between March and May and they coincide with more
359 depleted $\delta^{18}\text{O}$ precipitation signals, consistent with the amount effect (Dansgaard, 1964).



360 Hence, the most negative $\delta^{18}\text{O}$ values in RN stalagmites reflect an increased rainfall amount,
361 as a consequence of ITCZ position close to N-NEB (Cruz et al., 2009; Utida et al., 2019).

362 A generally drier climate prevailed in NEB after the 4.2 ky BP (Before Present) event
363 in the Mid-Holocene, which led to the development of a sparse vegetation cover, the
364 Caatinga (De Oliveira et al., 1999; Utida et al., 2020; Chiessi et al., 2021). These conditions
365 favored soil erosion during rainfall events and reduced soil thickness (Utida et al., 2020).
366 When erosion events remove most of the soil cover, there is an increase in the carbon
367 contribution from local bedrock (mean $\delta^{13}\text{C}$ of 0.5 ‰), which leads to higher $\delta^{13}\text{C}$ values in
368 the stalagmites (Utida et al., 2020). On the other hand, more negative $\delta^{13}\text{C}$ values in
369 stalagmites are associated with increased soil coverage and soil production. In NEB soils
370 have a $\delta^{13}\text{C}$ average around -25 ‰, which suggests a dominant influence from C3 plants
371 with $\delta^{13}\text{C}$ values ranging between -32‰ and -20‰ (Pessenda et al., 2010). Therefore, the
372 $\delta^{13}\text{C}$ stalagmite results are interpreted as changes in soil production/erosion and the density
373 of vegetation coverage (e.g., Utida et al., 2020; Azevedo et al., 2021; Novello et al., 2021).

374



375

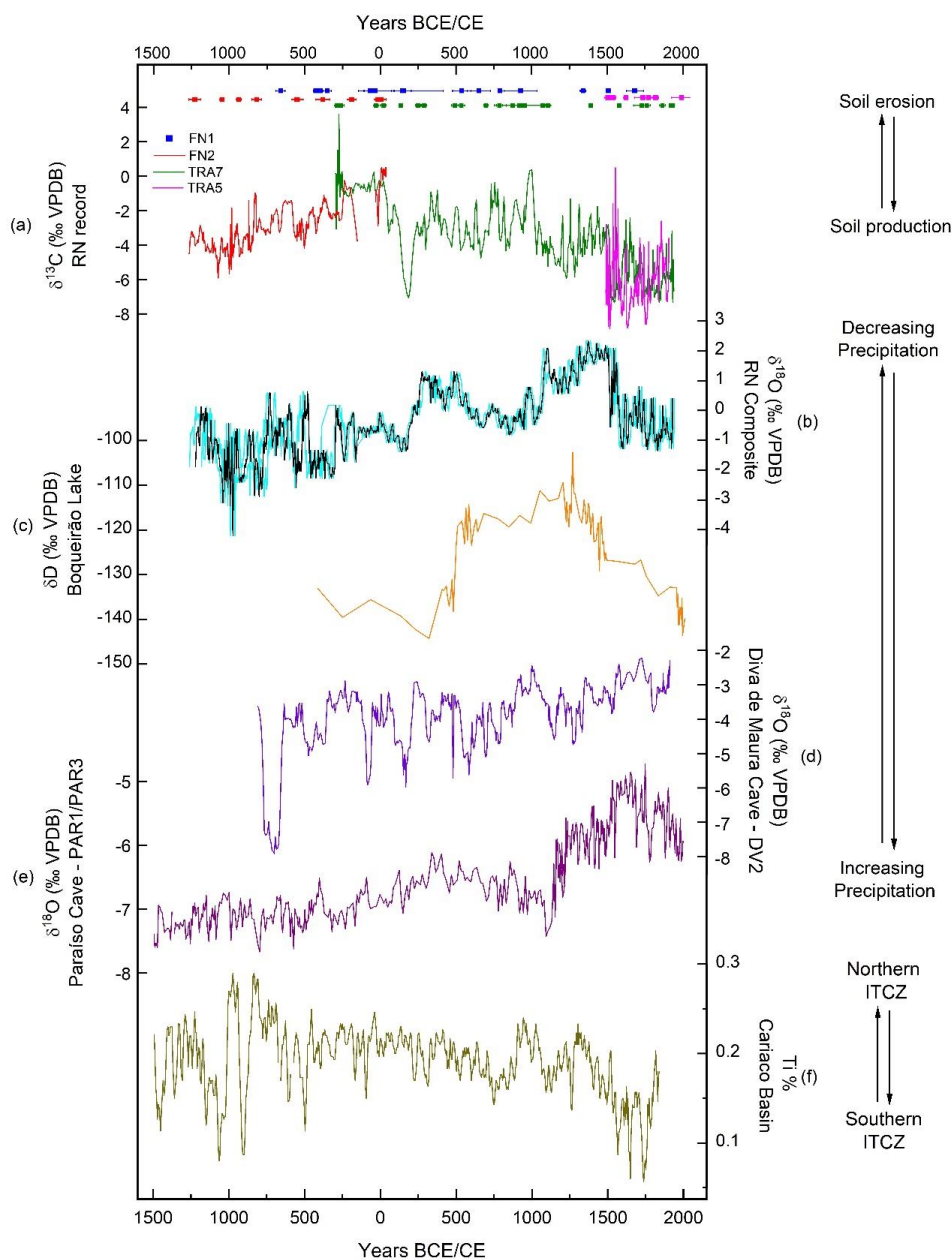
376 Figure 3 – Rio Grande do Norte stalagmite isotope record. a) Raw data of $\delta^{13}\text{C}$. (b)

377 Oxygen isotope results corrected for calcite-aragonite fractionation ($\delta^{18}\text{O}_{\text{C-A}}$), according to

378 weight proportion of mineralogical results. c) $\delta^{18}\text{O}$ composite constructed using stalagmite

379 records from NEB (black line). Cyan lines denote the age model confidence interval of

380 99%. Dots with error bars are U/Th ages of each stalagmite, according to their color.



381

382 Figure 4 – Comparison of a composite record of: a) carbon isotope ratios and b)

383 oxygen ratios obtained from RN stalagmites. Cyan lines denote confidence interval of 99%.

384 Colored squares are speleothem U/Th age results. c) Boqueirão Lake δD record (Utida et



385 al., 2019). d) DV2 speleothem oxygen isotope record from Diva de Maura cave, southern
386 NEB (Novello et al., 2012). e) PAR01 and PAR03 $\delta^{18}\text{O}$ records from Paraíso cave, eastern
387 Amazon (Wang et al., 2017). f) Ti record of Cariaco Basin (Haug et al., 2001).

388

389 The oldest period covered by the RN Composite, from 1060 to 480 BCE, reflects
390 increased precipitation in N-NEB as suggested by negative $\delta^{18}\text{O}$ anomalies during most of
391 this period, although a tendency from lower to higher $\delta^{13}\text{C}$ values is observed, possibly led
392 by surface soil erosion (Fig 4). This period is also characterized by successive dry and wet
393 multidecadal periods that could favor soil production but did not contribute much to the
394 carbon isotopic composition of speleothems because it was eroded during drier years, as
395 described in Utida et al. (2020). The association of erosion processes with $\delta^{13}\text{C}$ is rather
396 clear from 480 BCE to 0 CE when their values reach the bedrock signature at about -1‰ to
397 $+1\text{‰}$, which was caused by intense ITCZ rainfall as suggested by the more negative values
398 of $\delta^{18}\text{O}$. During the following period, the $\delta^{13}\text{C}$ values are slightly more negative but still high
399 from 200 CE to 1500 CE, when the climate was mostly dry. This relationship is contrary to
400 what is observed in the last 500 years, during the period equivalent to the Little Ice Age (LIA)
401 (here from 1500 to 1800 CE) and in the last two centuries, that is marked by very negative
402 values of $\delta^{13}\text{C}$ in response to wet climatic conditions as indicated by lower $\delta^{18}\text{O}$ values. The
403 more negative $\delta^{13}\text{C}$ during the LIA are probably related to denser vegetation that favored
404 both soil production and stability above the cave. Due to the high range of $\delta^{13}\text{C}$ results (more
405 than 11‰), we assumed that the Prior Calcite Precipitation effect would be negligible in our
406 results. In addition, the more positive $\delta^{13}\text{C}$ signal occur around 280 BCE when the climate
407 conditions were not the driest in the last 5000 years.

408 During the last 2500 years, the RN Composite shows similar characteristics as the
409 lower-resolution δD lipids obtained in Boqueirão Lake sediments (Fig 1 and 4). From 500 to



410 1500 CE, enriched δD lipids obtained in Boqueirão Lake sediments (N-NEB) were
411 interpreted as the beginning of a long dry phase (Utida et al., 2019), although the beginning
412 of the dry period is slightly delayed when compared with the RN speleothem isotope record.
413 This difference might be related to a strong influence of eolian and fluvial sedimentary
414 dynamics in Boqueirão Lake. Furthermore, the later location might also be affected by
415 different climatic conditions given its location in the eastern coastal sector of NEB (Zular et
416 al., 2018; Utida et al., 2019).

417 It is important to note that the RN record exhibits a climatic signal that is distinctly
418 different from the from DV2 speleothem record from Diva de Maura Cave in S-NEB (Novello
419 et al., 2012). The general trend toward more positive values seen in both stalagmites,
420 resulting from insolation forcing (Cruz et al., 2009; Novello et al., 2012), explains the
421 persistent dry conditions in the entire NEB region since 4.2 BP. However, the DV2 record
422 does not document the same multidecadal and centennial-scale climate variability as
423 recorded in the RN speleothem record (Fig 4). As demonstrated by the spatial correlation
424 maps between $\delta^{18}O$ values and regional precipitation (Fig 2), the S-NEB and N-NEB regions
425 are influenced by distinct rainfall regimes whose peaks of precipitation arise during the
426 summer monsoon season and the autumn ITCZ, respectively. Our data provide evidence
427 for this interpretation of differences in seasonality in northeastern Brazil during the last
428 millennia.

429 When considering conditions over the eastern Amazon, we see that the RN
430 Composite shares some similarities with the Paraiso stalagmite record, but there are also
431 important differences (Wang et al., 2017) (Fig 4). From the $\delta^{18}O$ peak around 250 CE to the
432 end of the drought period near 1500 CE, precipitation in both areas seems to share many
433 similar characteristics, assumed to be mostly driven by the ITCZ (Fig. 1). However, during
434 the event around 1100 CE, centered in the Medieval Climate Anomaly (MCA), and the period
435 from 1500 to 1750 CE, Paraiso is antiphased with the RN record and in phase with the



436 Cariaco Basin (Haug et al., 2001), which suggests a zonal behavior of precipitation shifts in
437 the ITCZ domain. Even though the Paraiso and Cariaco sites are located in different
438 hemispheres, the observed in-phase climate relationship during the LIA suggests that their
439 isotopic signatures were both sensitive to the same rainfall changes over northern South
440 America (Fig 2).

441 The Bond 2 Event is recorded in the RN Composite, marked by increased
442 precipitation around 1000 BCE, when the ITCZ was displaced toward the south. This
443 southerly ITCZ displacement might be attributed to persistent lower temperatures in the
444 North Atlantic (Bond et al., 2001; Broccoli et al., 2006) caused by the slowdown of the
445 Atlantic Meridional Overturning Circulation (Jackson et al., 2015).

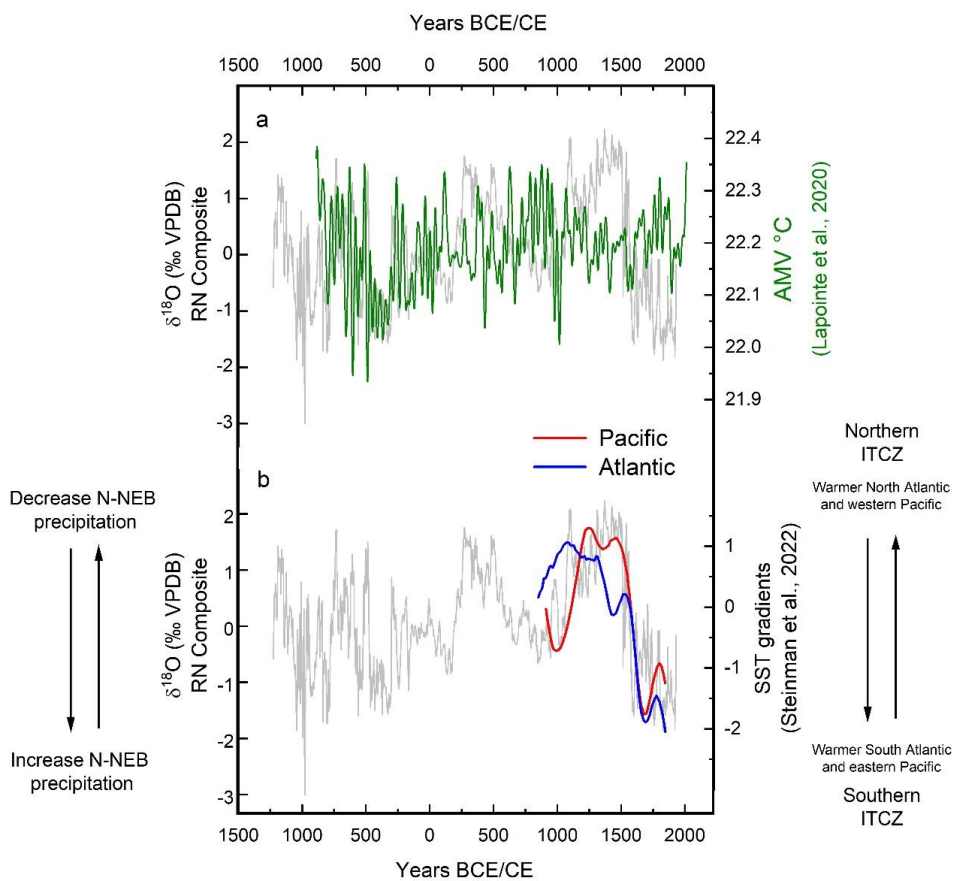
446 There is a relationship between the $\delta^{18}\text{O}$ values in our RN speleothems and Atlantic
447 Multidecadal Variability (AMV) (Lapointe et al., 2020), which reinforces the idea of an ITCZ
448 displacement toward the warmer hemisphere (Fig 5). Studies suggest that warm AMV forces
449 the ITCZ to shift meridionally (Knight et al., 2006, Levine et al., 2018), while model
450 simulations also suggest weakening of ITCZ from February to July during warm AMV
451 (Maksic et al., 2022). Although there are some decoupling intervals between our results and
452 the AMV during the last two millennia, the driest periods from 200 to 580 CE and 1100 and
453 1500 CE occurred during long relatively warm AMV anomalies which would force a
454 northward ITCZ displacement and low precipitation variability over NEB.

455 Analyzed observed precipitation anomaly patterns during the mean states defined
456 by the overlapping periods of AMV and Pacific Decadal Variability (PDV) show that dry
457 conditions over N-NEB and eastern Amazon are present when both AMV and PDV are in
458 warm phases, or when AMV is cold and PDV is in warm phases (Kayano et al., 2020, 2022).
459 On the other hand, when AMV and PDV are both in cold phase, precipitation over Amazon
460 is anti-phased with NEB, resulting in decreased precipitation over the Amazon and
461 increased precipitation over NEB. Our analysis corroborates with this and points to



462 increasing precipitation over N-NEB and decreasing precipitation over eastern Amazon,
463 between 1500 and 1750 CE, when both AMV and PDV are in cold phase (Fig 4). This sign
464 reversal is assigned to perturbations of the regional Walker cell's produced by
465 teleconnection between the Atlantic and Pacific (Kayano et al., 2022, He et al., 2021).

466 Steinmann et al. (2022), suggested a southward displacement of the ITCZ during the
467 Common Era toward the southern hemisphere in response to changes in the Pacific and
468 Atlantic meridional SST gradients. Indeed, our RN Composite is dynamically consistent with
469 these SST gradient changes and in agreement with the hypothesis of a north-south
470 oscillation of the latitudinal ITCZ position in the tropical Atlantic during the last millennia,
471 modulating precipitation over N-NEB. When the tropical South Atlantic and tropical eastern
472 Pacific are anomalously warm (cold) the ITCZ is displaced to the south (north), resulting in
473 increasing (decreasing) precipitation over NEB, as observed during the LIA (Fig 5). The
474 abrupt changes in N-NEB precipitation around 1100 and 1500 CE occur approximately
475 synchronous with the SST gradient changes, confirming how sensitive the RN speleothems
476 respond to changes in the ITCZ latitudinal position (Fig 5). According to Steinmann et al.
477 (2022), during the LIA period warm SST in the eastern tropical Pacific and in the tropical
478 South Atlantic would promote a southward displacement of the ITCZ. This is supported by
479 other records from the western Amazon and the tropical Andes that document an intensified
480 SASM during the LIA, fueled by the southern location of the ITCZ (e.g., Vuille et al., 2012;
481 Apaéstegui et al., 2018), which is also very well recorded in other archives around the tropics
482 (Leichtleitner et al., 2017; Campos et al., 2019; Orrison et al., 2022; Steinmann et al., 2022).



483

484 Figure 5 - $\delta^{18}\text{O}$ RN Composite compared with (a) Atlantic Multidecadal Variability

485 (Lapointe et al., 2020) and (b) Pacific and Atlantic Sea Surface Temperature gradients

486 calculated according to Steinman et al. (2022). Atlantic: 2σ range of 1,000 realizations of the

487 Atlantic meridional SST gradient (north – south). Pacific: median of 1,000 realizations of the

488 Pacific zonal SST gradient (west – east).

489

490 5.2. The use of RN $\delta^{18}\text{O}$ as a recorder of extreme dry events

491



492 In NEB, the low water availability has been one of the major challenges faced by its
493 people during the last centuries (Marengo and Bernasconi, 2015; Marengo et al., 2021; Lima
494 and Magalhães, 2018). On the other hand, the last 500 years were the wettest of the last
495 two millennia, according to our results (Fig 4). Superimposed on these long-term negative
496 $\delta^{18}\text{O}$ anomalies, distinct peaks are recorded in the higher resolution TRA5 $\delta^{18}\text{O}$ record from
497 1500 to 1850 CE (Fig 6). The highest peaks correspond to extreme drought events, such as
498 the ones centered around 1546 and 1564 CE (points 1 and 2 of Fig 6). They can be
499 associated with observed historical droughts that took place in 1553 and 1559 CE. These
500 were the first two events recorded in Brazil by the Portuguese Jesuits that led to a reported
501 reduction in riverflow in the tributaries of the main rivers of NEB (Serafim Leite, 1938; Hue
502 et al., 2006; Lima and Magalhães, 2018).

503 Another relevant drought according to TRA5 is centered around 1620 CE (point 3 of
504 Fig 6). This drought is recorded in historical documents and lasted from 1614 to 1615 CE,
505 although it did not have the same socioeconomic impact as the two prior droughts (Lima
506 and Magalhães, 2018). In fact, from the middle of the 16th to the middle of the 17th century
507 there are few historical drought records (point a of Fig 6). One hypothesis to explain this
508 hiatus is the low population density of the NEB territory, resulting in poor historical
509 documentation of such events. However, according to the TRA5 record, between the event
510 2 ~1564 CE and event 4 ~1717 CE (Fig 6), the only drought peak occurs in 1620 CE,
511 confirming an almost 150-year long period of relative climate stability with prevailing wet
512 conditions in NEB. These favorable conditions certainly helped with the initial population
513 establishment at the beginning of 16th century, and led to the peak era of sugar cane
514 production in NEB around 1650 CE along coastal areas (Taylor, 1970).

515 During the 18th century NEB experienced a significant increase in rural population,
516 characterized by the establishment of large cattle farms (Fausto, 2006). In this period, three
517 droughts are documented in the TRA5 record (Fig 6). The $\delta^{18}\text{O}$ excursion around 1717 CE



518 (point 4 in Fig 6) can be associated with the drought that lasted from 1720 to 1727 CE; the
519 first big drought in NEB, which according to historical documents, caused the mortality of
520 wildlife and cattle, and affected the agricultural productivity. Entire indigenous tribes died of
521 starvation as a consequence of this drought and a related smallpox (variola) epidemic, which
522 also killed other ethnic groups, especially the native population and black people enslaved
523 during that period (Alves, 1929).

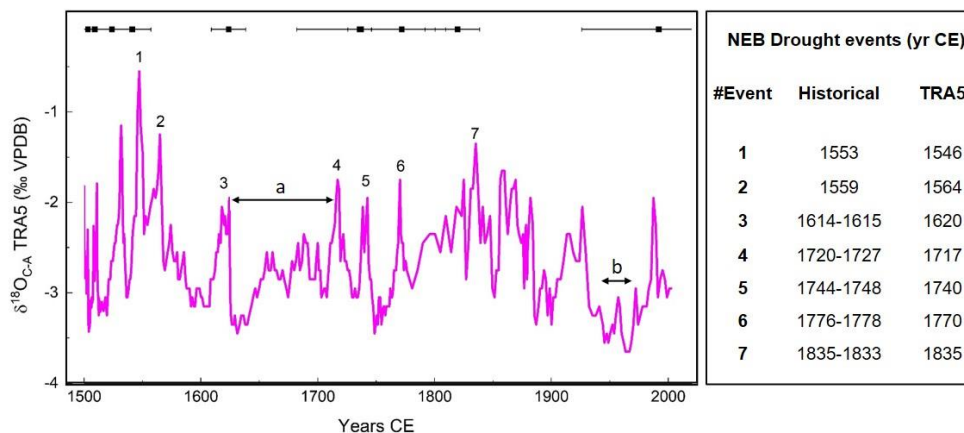
524 The following event around 1740 CE (point 5 in Fig 6) was also recorded in historical
525 documents, but did not seem to be associated with major impacts. However, all of these
526 droughts were probably responsible for a drop in sugar-cane exports to Europe during the
527 first half of the 18th century (Galloway, 1975).

528 Another drought occurred from 1776 to 1778 CE, and is imprinted in our record
529 around 1770 CE (point 6 in Fig 6). This event was again accompanied by a variola outbreak
530 probably spread by lowering in sanitary conditions and increased people agglomeration. The
531 association between this disease and droughts might explain the economic and health crisis,
532 since people started to migrate to the cities looking for treatment and food, leading the
533 Governor to transfer infected people to isolated lands, resulting in thousands of deaths
534 (Rosado, 1981). Finally, the most recent peak in our data displays an event around 1835
535 CE (point 7 of Fig 6), associated with a drought that lasted from 1833 to 1835, reaching the
536 northernmost areas of NEB, and leading to the largest human migration to other Brazilian
537 regions (Lima and Magalhães, 2018).

538 Our TRA5 stalagmite data record some of the most important droughts that occurred
539 in NEB between the 16th and the 18th centuries, demonstrating the potential of stalagmite
540 studies in monitoring abrupt and extreme climate events through time. However, the
541 speleothems do not record all documented historical dry events, as some droughts may not
542 have affected the Trapiá Cave region or they were not strong or long enough to affect the
543 isotopic signal of the groundwater storage in the epikarst.



544 Although the TRA5 speleothem chronology is not so precise during the last ~150
545 years, we observe that the wet period from 1940s to 1970s (point b of Fig 6) is coincident
546 with the mid-20th Century break in global warming that has been discussed to be forced by
547 aerosol emissions (e.g., Booth et al., 2012; Undorf et al., 2018). Our data suggest an
548 increased precipitation in this period that is supported by a trend in decreasing values of
549 $\delta^{18}\text{O}$ in corals from the northeast coast of N-NEB that is interpreted as an ITCZ southward
550 displacement caused by decreasing SST gradient between North and South Atlantic
551 (Pereira et al., 2022).



552
553 Figure 6 – $\delta^{18}\text{O}_{\text{C-A}}$ record from TRA5 speleothem and its U/Th ages and errors
554 represented by black dots and lines at the top of the graph. The numbers in the graph
555 represent the occurrence of historical drought years compiled from Lima and Magalhães
556 (2018). a - middle of the 16th to the middle of the 17th century. b - 1940s to 1970s period.

557

558 6. Conclusions

559

560 We present the first high-resolution record for the ITCZ in N-NEB that covers the last
561 3200 years and also records the major historical droughts that took place in NEB during the



562 last 500 years. Based on two distinct proxies, we describe the regions' paleoclimate
563 variability for the last 2500 years and its connections to remote forcing mechanisms such as
564 the AMV and changes in Pacific and Atlantic SST gradients.

565 The N-NEB record presents a trend toward drier conditions as is also being observed
566 in the Diva de Maura Cave in S-NEB, interpreted as an ITCZ withdrawal and SASM
567 weakening, respectively. These data suggest a trend toward increased aridity over NEB
568 from 3000 BP to the present, although the two records are influenced by distinctly different
569 climate systems with different precipitation seasonality.

570 During the last millennia, ITCZ dynamics in the tropical Atlantic – South America
571 sector cannot be explained solely by north-south ITCZ migrations or one single forcing
572 mechanism. We propose a zonally non-uniform behavior of the ITCZ during the event
573 centered around 1100 CE and the drought period between 1500 and 1750 CE, when the
574 RN record is anti-phased with the Paraiso cave record from the eastern Amazon. This zonal
575 behavior would be forced by the interactions between AMV and PDV modes that changed
576 the regional Walker cell position and ITCZ intensity/width and thus affecting precipitation
577 variability between eastern Amazon and N-NEB.

578 The historical droughts recorded in the RN stalagmite suggest that much of the
579 socioeconomic development of the NEB, which occurred after 1500 CE, benefitted from
580 conditions that were unusually humid in a long-term context. During the last 500 years the
581 technological development, infrastructure, civilization and population growth relied on more
582 abundant resources. On the other hand, our data also shows how short, abrupt drought
583 events significantly affected human population and other life forms, especially when
584 associated with anthropogenic changes in the environment. These droughts induced an
585 environment favorable for spreading of disease, starvation, lack of water, environmental
586 degradation and crowding of people seeking help, among other problems. These events
587 demonstrate the social and environmental impacts associated with extreme events in this



588 vulnerable environment and our speleothem work documents the enormous potential of
589 these archives to reconstruct the drought history in this region.

590

591 *Acknowledgments*

592 We thank Alyne Barros M. Lopes, Osmar Antunes and Christian Millo (LES-IGC-
593 USP, Brazil) for their support during the analyses. We thank M.E.D.-L.G, J.C.R., E.A.S.B,
594 V.A. and W.D. for their support in U/Th analysis. We are grateful to Leda Zogbi and Diego
595 de Medeiros Bento for the Trapiá cave and Furna Nova maps. We thank Jocy Brandão Cruz,
596 Diego de Medeiros Bento, José Iatagan Mendes de Freitas, Darcy José dos Santos, Uilson
597 Paulo Campos (CECAV/RN), Antônio Idaelson do Nascimento and Geilson Góes
598 Fernandes for all support in the field trip, information and data about the caves. This work
599 was supported by the FAPESP, Brazil through PIRE NSF-FAPESP [2017/50085-3 to
600 F.W.C], as well as the fellowships to G.U. [2020/02737-4], V.F.N [2016/15807-5], J.M.
601 [2018/23522-6] and A.A. [2020/09258-4]. The NSF, United States support through grants
602 [AGS-1303828 and OISE-1743738] to MV and 1103403 to R.L.E and H.C. is acknowledged.
603 The NSFC, China support through grant [NSFC 41888101] to H.C. and [NSFC
604 42261144753] to H.Z. is acknowledged, G.U. is grateful to CAPES for the PhD and PosDoc
605 fellowships through the Programa de Pós-Graduação em Geoquímica e Geotectônica at
606 Universidade de São Paulo, Brazil.

607



608 *References*

609

610 Alvalá, R.C.S., Cunha, A.P.M.A., Briton, S.S.B., Seluchi, M.E., Marengo, J.A., Moraes,
611 O.L.L., Carvalho, M.A.: Drought monitoring in the Brazilian Semiarid region, An. Acad.
612 Bras. Ciênc., 91 (1), e20170209, <https://doi.org/10.1590/0001-3765201720170209>,
613 2019.

614 Alves, J.: História das secas (século XVII a XIX). Fundação Waldemar Alcântara, Fortaleza,
615 [https://colecaomossoroense.org.br/site/wp-](https://colecaomossoroense.org.br/site/wp-content/uploads/2018/07/HIST%C3%93RIA-DAS-SECAS.pdf)
616 [content/uploads/2018/07/HIST%C3%93RIA-DAS-SECAS.pdf](https://colecaomossoroense.org.br/site/wp-content/uploads/2018/07/HIST%C3%93RIA-DAS-SECAS.pdf), last access: 22 March
617 2022. 2003.

618 ANA – Agência Nacional de Águas, Sistema Nacional de Informações sobre Recursos
619 Hídricos: <http://www.snirh.gov.br/hidroweb/apresentacao>, last access: 01 February
620 2022, 2013.

621 Andreoli, R. F. S., de Souza, R.A.F., Kayano, M.T., Candido, L.A.: Seasonal anomalous
622 rainfall in the central and eastern Amazon and associated anomalous oceanic and
623 atmospheric patterns, Int. J. Climatol., 32, 1193–1205, <https://doi.org/10.1002/joc.2345>,
624 2011.

625 Apaéstegui, J., Cruz, F.W., Vuille, M., Fohlmeister, J., Espinoza, J.C., Sifeddine, A., Strikis,
626 N., Guyot, J.L., Ventura, R., Cheng, H., Edwards, R.E.: Precipitation changes over the
627 eastern Bolivian Andes inferred from speleothem ($\delta^{18}\text{O}$) records for the last 1400 years,
628 Earth Planet. Sci. Lett., 494, 124–134, <https://doi.org/10.1016/j.epsl.2018.04.048>, 2018.

629 Araújo, R.G., Andreoli, R.V., Candido, L.A., Kayano, M.T., de Souza, R.A.F.: Influence of El
630 Niño-Southern Oscillation and Equatorial Atlantic on rainfall over northern and
631 northeastern regions of South America, Acta Amaz., 43, 4, 469-480,
632 <https://doi.org/10.1590/S0044-59672013000400009>, 2013.



- 633 Azevedo, V., Strikis, N.M., Novello, V.F., Roland, C.L., Cruz, F.W., Santos, R.V., Vuille, M.,
634 Utida., G., de Andrade, F.D., Cheng, H., Edwards, R.L.: Paleovegetation seesaw in
635 Brazil since the Late Pleistocene: A multiproxy study of two biomes, *Earth Planet. Sci.*
636 *Lett.*, 563, 116880, <https://doi.org/10.1016/j.epsl.2021.116880>, 2021.
- 637 Bond, G., Kromer, B., Beer, Muscheler, R., Evans, M.N., Showers, W., Hoffmann, S., Lotti-
638 Bond, R., Hajdas, I., Bonani, G.: Persistent Solar Influence on North Atlantic Climate
639 During the Holocene, *Science*, 294, 2130-2136,
640 <https://doi.org/10.1126/science.1065680>, 2001.
- 641 Booth, B.B.B., Dunstone, N.J., Halloran, et al., P.R., Andrews, T., Bellouin, N.: Aerosols
642 implicated as a prime driver of twentieth-century North Atlantic climate variability, *Nature*,
643 484, 228-232, <https://doi.org/10.1038/nature10946>, 2012.
- 644 Breitenbach, S.F.M., Rehfeld, K., Goswami, B., Baldini, J.U.L., Ridley, H. E., Kennett, D. J.,
645 Prufer, K.M., Aquino, V.V., Asmerom, Y., Polyak, V.J., Cheng, H., Kurths, J., Marwan,
646 N.: COConstructing Proxy Records from Age models (COPRA), *Clim. Past*, 8, 1765–1779,
647 <https://doi.org/10.5194/cp-8-1765-2012>, 2012.
- 648 Broccoli, A. J., Dahl, K.A., Stouffer, R.J.: Response of the ITCZ to Northern Hemisphere
649 cooling, *Geophys. Res. Lett.*, 33, L01702, <https://doi.org/10.1029/2005GL024546>, 2006.
- 650 Campos, J.L.P.S., Cruz, F.W., Ambrizzi, T., Deininger, M., Vuille, M., Novello, V.F., Strikis,
651 N.M.: Coherent South American Monsoon Variability During the Last Millennium
652 Revealed Through High-Resolution Proxy Records, *Geophys. Res. Lett.*, 46, 8261–
653 8270, <https://doi.org/10.1029/2019GL082513>, 2019.
- 654 Cheng, H., Edwards, R.L., Shen, C-C., Polyak, V.J., Asmerom, Y., Woodhead, J.,
655 Hellstrom, J., Wang, Y., Kong, X., Spötl, C., Wang, X., Alexander Jr. E.C.:
656 Improvements in ^{230}Th dating, ^{230}Th and ^{234}U half-life values and U-Th isotopic
657 measurements by multi-collector inductively coupled plasma mass spectrometry, *Earth*
658 *Planet. Sci. Lett.*, 371-372, 82-91, <https://doi.org/10.1016/j.epsl.2013.04.006>, 2013.



- 659 Chiessi, C. M., Mulitza, S., Taniguchi, N.K., Prange, M., Campos, M.C., Häggi, C., Schefuß,
660 E., Pinho., T.M.L., Frederichs, T., Portilh-Ramos, R.C., Souza, S.H.M., Crivellari, S.,
661 Cruz, F.W.: Mid- to late-Holocene contraction of the Intertropical Convergence Zone over
662 northeastern South America, *Paleocean. Paleoclim.*, 36, e2020PA003936,
663 <https://doi.org/10.1029/2020PA003936>, 2021.
- 664 Cruz, F.W., Vuille, M., Burns, S.J., Wang, X., Cheng, H., Werner, M., Edwards, R.L.,
665 Karman, I., Auler, A.S., Nguyen, H.: Orbitally driven east-west antiphasing of South
666 American precipitation, *Nat. Geosci.*, 2, 210-214, <https://doi.org/10.1038/ngeo444>,
667 2009.
- 668 Dansgaard, W.: Stable isotopes in precipitation, *Tellus XVI*, 4, 436-468,
669 <https://doi.org/10.1111/j.2153-3490.1964.tb00181.x>, 1964.
- 670 De Oliveira, P.E., Barreto, A.M.F., Suguio, K.: Late Pleistocene-Holocene climatic and
671 vegetational history of the Brazilian Caatinga: the fossil dunes of the middle São
672 Francisco River, *Palaeogeogr. Palaeoclimatol. Palaeoecol.*, 152, 319-337,
673 [https://doi.org/10.1016/S0031-0182\(99\)00061-9](https://doi.org/10.1016/S0031-0182(99)00061-9), 1999.
- 674 Della Libera, M.E., Novello, V.F., Cruz, F.W., Orrison, R., Vuille, M., Maezumi, S.Y., de
675 Souza, J., Cauhy, J., Campos, J.L.P.S., Ampuero, A., Utida., G., Stríkis, N.M., Stumpf,
676 C.F., Azevedo, V., Zhang, H., Edwards, R.L., Cheng, H.: Paleoclimatic and
677 paleoenvironmental changes in Amazonian lowlands over the last three millennia, *Quat.*
678 *Sci. Rev.*, 279, 107383, <https://doi.org/10.1016/j.quascirev.2022.107383>, 2022.
- 679 Erasmi, S., Maurer, F., Petta, R.A., Gerold, G., Barbosa, M.P.: Interannual variability of the
680 Normalized Difference Vegetation Index over Northeast Brazil and its relation to rainfall
681 and El Niño Southern Oscillation, *Geo-Öko*, 30, 3-4, 185-206, 2009.
- 682 Fausto, B.: *História do Brasil*, 12th ed., Editora Universidade de São Paulo, São Paulo, 660
683 pp., ISBN 85-314-0240-9, 2006.



- 684 Fohlmeister, J.: A statistical approach to construct composite climate records of dated
685 archives, *Quat. Geochronol.*, 14, 48-56, <https://doi.org/10.1016/j.quageo.2012.06.007>,
686 2012.
- 687 Galloway, J.H.: Northeast Brazil 1700-50: The agricultural crisis re-examined, *J. Hist.*
688 *Geogr.*, 1, 1, 21-38, [https://doi.org/10.1016/0305-7488\(75\)90073-0](https://doi.org/10.1016/0305-7488(75)90073-0), 1975.
- 689 Gomes, H.B., Ambrizzi, T., Herdies, D.L., Hodges, K., da Silva, B.F.P.: Easterly Wave
690 Disturbances over Northeast Brazil: An Observational Analysis, *Adv. Meteorol.*, 176238,
691 <https://doi.org/10.1155/2015/176238>, 2015.
- 692 Grazulis, S., Chateigner, D., Downs, R.T., Yokochi, A.F.T., Quirós, M., Lutterotti, L.,
693 Manakova, E., Butkus, J., Moeck, P., Le Bail, A.: Crystallography Open Database – an
694 open-access collection of crystal structures, *J. Appl. Crystallogr.*, 42, 726-729,
695 <https://doi.org/10.1107/S0021889809016690>, 2009.
- 696 Haug, G., Hughen, K.A., Sigman, D.M., Peterson, L.C., Röhl, U.: Southward migration of the
697 Intertropical Convergence Zone through the Holocene, *Science*, 293, 5533, 1304-1308,
698 <https://doi.org/10.1126/science.1059725>, 2001.
- 699 He, Z., Dai, A., Vuille, M.: The Joint Impacts of Atlantic and Pacific Multidecadal Variability
700 on South American Precipitation and Temperature, *J. Clim.*, 34, 7959-7981,
701 <https://doi.org/10.1175/JCLI-D-21-0081.1>, 2021.
- 702 Hue, S. M.: *Primeiras Cartas do Brasil 1551-1555: Introdução e notas*, Jorge Zahar Editor,
703 Rio de Janeiro, 147 pp., ISBN 8571109079, 2006.
- 704 IAEA/GNIP - Global Network of Isotopes in Precipitation, The GNIP Database,
705 <https://nucleus.iaea.org/wiser>, last access: 20 August 2021.
- 706 INMET - Instituto Nacional de Meteorologia, Banco de Dados Meteorológicos para Ensino
707 e Pesquisa, <http://www.inmet.gov.br/>, last access 5 November 2021.
- 708 Jackson, L. C., Kahana, R., Graham, T., Ringer, M.A., Woollings, T., Mecking, J.V., Wood,
709 R.A.: Global and European climate impacts of a slowdown of the AMOC in a high



- 710 resolution GCM, *Clim. Dyn.*, 45, 3299–3316, [https://doi.org/10.1007/s00382-015-2540-](https://doi.org/10.1007/s00382-015-2540-2)
711 2, 2015.
- 712 Kayano, M.T., Andreoli, R.V., de Souza, R.A.: Pacific and Atlantic multidecadal variability
713 relations to the El Niño events and their effects on the South American rainfall, *Int. J.*
714 *Clim.*, 40(4), 2183-2200, <https://doi.org/10.1002/joc.6326>, 2020.
- 715 Kayano, M.T., Cerón, W.L., Andreoli, R.V., Souza, R.A.F., Avila-Diaz, A., Zuluaga, C.F.,
716 Carvalho, L.M.V.: Does the El Niño-Southern Oscillation Affect the Combined Impact of
717 the Atlantic Multidecadal Oscillation and Pacific Decadal Oscillation on the Precipitation
718 and Surface Air Temperature Variability over South America?, *Atmos.*, 13, 231,
719 <https://doi.org/10.3390/atmos13020231>, 2022.
- 720 Knight, J.R., Folland, C.K., Scaife, A.A.: Climate impacts of the Atlantic Multidecadal
721 Oscillation, *Geophys. Res. Lett.*, 33, L17706, <https://doi.org/10.1029/2006GL026242>,
722 2006.
- 723 Lapointe, F., Bradley, R.S., Francus, P., Balascio, N.L., Abbott, M.B., Stoner, J.S., St-Onge,
724 G., De Coninck, A., Labarre, T.: Annually resolved Atlantic Sea surface temperature
725 variability over the past 2,900 y, *PNAS*, 117, 44, 27171–27178,
726 <https://doi.org/10.1073/pnas.2014166117>, 2020.
- 727 Lechleitner, F. A., Breitenbach, S.F.M., Rehfeld, K., Ridley, H.E., Asmerom, Y., Prufer, K.M.,
728 Marwan, N., Goswami, B., Kennett, D.J., Aquino, V.V., Polyak, V., Haug, G.H., Eglinton,
729 T.I., Baldini, J.U.L.: Tropical rainfall over the last two millennia: Evidence for a low-
730 latitude hydrologic seesaw, *Sci. Rep.*, 7, 45809, <https://doi.org/10.1038/srep45809>,
731 2017.
- 732 Lenters, J. D., Cook, K. H.: On the origin of the Bolivian High and related circulation features
733 of the South American climate, *J. Atmos. Sci.*, 54, 656–677,
734 [https://doi.org/10.1175/1520-0469\(1997\)054<0656:OTOOTB>2.0.CO;2](https://doi.org/10.1175/1520-0469(1997)054<0656:OTOOTB>2.0.CO;2), 1977.



- 735 Levine, A.F.Z., Frierson, D.M.W., McPhaden, M.J.: AMO Forcing of Multidecadal Pacific
736 ITCZ Variability, *J. Clim.*, 31, 5749–5764, <https://doi.org/10.1175/JCLI-D-17-0810.1>,
737 2018.
- 738 Lima, J.R., Magalhães, A.R.: Secas no Nordeste: registros históricos das catástrofes
739 econômicas e humanas do século 16 ao século 21, *Parcer. Estratég.*, 23, 46, 191-212,
740 2018.
- 741 Maksic J., Shimizu, M.H., Kayano, M.T., Chiessi, C.M., Prange, M., Sampaio, G.: Influence
742 of the Atlantic Multidecadal Oscillation on South American Atmosphere Dynamics and
743 Precipitation, *Atmos.*, 13, 11, 1778, <https://doi.org/10.3390/atmos13111778>, 2022.
- 744 Marengo, J.A., Bernasconi, M.: Regional differences in aridity/drought conditions over
745 Northeast Brazil: present state and future projections, *Clim. Chang.*, 129, 103-115,
746 <https://doi.org/10.1007/s10584-014-1310-1>, 2015.
- 747 Marengo, J.A., Galdos, M.V., Challinor, A., Cunha, A.P., Marin, F.R., Vianna, M.S., Alvala,
748 R.C.S., Alves, L.M., Moraes, O.L., Bender, F.: Drought in Northeast Brazil: A review of
749 agricultural and policy adaptation options for food security, *Clim. Resil. Sustain.*, 1, 17,
750 <https://doi.org/10.1002/cli2.17>, 2021.
- 751 Melo, A.C.C., Castro, D.L., Bezerra, F.H.R., Bertotti, G.: Rift fault geometry and evolution in
752 the Cretaceous Potiguar Basin (NE Brazil) based on fault growth models, *J. South Am.*
753 *Earth Sci.*, 71, 96-107, <https://doi.org/10.1016/j.jsames.2016.07.006>, 2016.
- 754 Novello, V.F., Cruz, F.W., Karmann, I., Burns, S.J., Stríkis, N.M., Vuille, M., Cheng, H.,
755 Edwards, R.L., Santos, R.V., Frigo, E., Barreto, E.A.S.: Multidecadal climate variability
756 in Brazil's Nordeste during the last 3000 years based on speleothem isotope records,
757 *Geophys. Res. Lett.*, 39, L23706, <https://doi.org/10.1029/2012GL053936>, 2012.
- 758 Novello, V.F., Cruz, F.W., Moquet, J.S., Vuille, M., de Paula, M.S., Nunes, D., Edwards,
759 R.L., Cheng, H., Karmann, I., Utida, U., Stríkis, N.M., Campos, J.L.P.S.: Two Millennia



- 760 of South Atlantic Convergence Zone Variability Reconstructed from Isotopic Proxies,
761 *Geophys. Res. Lett.*, 45, <https://doi.org/10.1029/2017GL076838>, 2018.
- 762 Novello, V.F., Cruz, F.W., Vuille, M., Campos, J.L.P.S., Stríkis, N.M., Apaéstegui, J.,
763 Moquet, J.S., Azevedo, V., Ampuero, A., Utida, G., Wang, X., Paula-Santos, G.M.,
764 Jaqueto, P., Pessenda, L.C.R., Breecker, D.O., Karmann, I.: Investigating $\delta^{13}\text{C}$ values
765 in stalagmites from tropical South America for the last two millennia, *Quat. Sci. Rev.*,
766 255, 106822, <https://doi.org/10.1016/j.quascirev.2021.106822>, 2021.
- 767 Orrison, R., Vuille, M., Smerdon, J.E., Apaéstegui, J., Azevedo, V., Campos, J.L.P.S., Cruz,
768 F.W., Della Libera, M.E., Stríkis, N.M.: South American Monsoon variability over the last
769 millennium in paleoclimate records and isotope-enabled climate models, *Clim. Past*, 18,
770 2045–2062, <https://doi.org/10.5194/cp-18-2045-2022>, 2022.
- 771 Paquette, J., Reeder, R.J.: Single-crystal X-ray structure refinements of two biogenetic
772 magnesian calcite crystals, *Am. Mineral.*, 75, 1151-1158, 1990.
- 773 Pereira, N.S., Clarke, L.J., Chiessi, C.M., Kilbourne, K.H., Crivellari, S., Cruz, F.W., Campos,
774 J.L.P.S., Yu, T.-L., Shen, C.-C., Kikuchi, R.K.P., Pinheiro, B.R., Longo, G.O., Sial, A.N.,
775 Felis, T.: Mid to late 20th century freshening of the western tropical South Atlantic
776 triggered by southward migration of the Intertropical Convergence Zone, *Palaeogeogr.*
777 *Palaeoclimatol. Palaeoecol.*, 597, 111013,
778 <https://doi.org/10.1016/j.palaeo.2022.111013>, 2022.
- 779 Pessenda, L.C.R., Gouveia, S.E.M., Ribeiro, A.S., De Oliveira, P.E., Aravena, R.: Late
780 Pleistocene and Holocene vegetation changes in northeastern Brazil determined from
781 carbon isotopes and charcoal records in soils, *Palaeogeogr. Palaeoclimatol. Palaeoecol.*
782 297, 597-608, <https://doi.org/10.1016/j.palaeo.2010.09.008>, 2010.
- 783 Pessoa-Neto, O.C.: Estratigrafia de sequências da plataforma mista neogênica na Bacia
784 Potiguar, margem equatorial brasileira, *Revista Bras. Geociênc.*, 33, 3, 263-278, 2003.



- 785 Pokroy, B., Fieramosca, J. S., Von Dreele, R. B., Fitch, A. N., Caspi, E. N., Zolotoyabko, E.:
786 Atomic structure of biogenic aragonite, *Chem. Mater.*, 19, 3244-3251,
787 <https://doi.org/10.1021/cm070187u>, 1989.
- 788 Rosado, J. V.-U., (org): Memorial da Seca. Brasília, Coleção Mossoroense, nº 163, Centro
789 Gráfico do Senado Federal/ESAM, [https://colecaomossoroense.org.br/site/acervo-](https://colecaomossoroense.org.br/site/acervo-oswaldo-lamartine/)
790 [oswaldo-lamartine/](https://colecaomossoroense.org.br/site/acervo-oswaldo-lamartine/), last access: 25 August 2022, 1981.
- 791 Sampaio, P.R.F., Saraiva Jr, J.C., Portela, J.C., da Silva, J.F.: Agricultural areas to
792 desertification in RN and mitigating measures: the case of settlements Milagres and
793 Terra da Esperança, *HOLOS*, 36, 7, e5902, <https://doi.org/10.15628/holos.2020.5902>,
794 2020.
- 795 Schneider, U., Becker, A., Finger, P., Meyer-Christoffer, A., Rudolf, B., Ziese, M.: GPCC
796 Full Data Reanalysis Version 6.0 at 1.0°: Monthly Land-Surface Precipitation from
797 Rain-Gauges built on GTS-based and Historic Data,
798 https://doi.org/10.5676/DWD_GPCC/FD_M_V7_100, 2011.
- 799 Schneider, T., Bischoff, T., Haug, G.H.: Migrations and dynamics of the intertropical
800 convergence zone, *Nature*, 513, 7516, 45-53, <https://doi.org/10.1038/nature13636>,
801 2014.
- 802 Serafim Leite, S.J.: História da Companhia de Jesus no Brasil, Tomo II (Século XVI - A
803 Obra), *Civilização Brasileira*, Rio de Janeiro, 658 pp. 1938.
- 804 Silva, O.L., Bezerra, F.H.R., Maia, R.P., Cazarin, C.L.: Karst landforms revealed at various
805 scales using LiDAR and UAV in semi-arid Brazil: Consideration on karstification
806 processes and methodological constraints, *Geomorphol.*, 295, 611-630,
807 <https://doi.org/10.1016/j.geomorph.2017.07.025>, 2017.
- 808 Steinman, B.A., Stansell, N.D., Mann, M.E., Cooke, C.A., Abbott, M.B., Vuille, M., Bird, B.W.,
809 Lachniet, M.S., Fernandez, A.: Interhemispheric antiphasing of neotropical precipitation



810 during the past millennium, PNAS, 119, 17, e2120015119,
811 <https://doi.org/10.1073/pnas.2120015119>, 2022.

812 Sulca, J., Vuille, M., Silva, Y., Takahashi, K.: Teleconnections between the Peruvian Central
813 Andes and Northeast Brazil during Extreme Rainfall Events in Austral Summer, J.
814 Hydrometeorol., 17, 499-515, <https://doi.org/10.1175/JHM-D-15-0034.1>, 2016.

815 Taylor, K.S.: The Economics of Sugar and Slavery in Northeastern Brazil, Agric. Hist., 44 3,
816 267-280, 1970.

817 Undorf, S., Bollasina, M.A., Hegerl, G.C.: Impacts of the 1900–74 Increase in Anthropogenic
818 Aerosol Emissions from North America and Europe on Eurasian Summer Climate, J.
819 Clim., 31, 8381-8399, <https://doi.org/10.1175/JCLI-D-17-0850.1>, 2018.

820 Utida, G., Cruz, F.W., Etourneau, J., Bouloubassi, I., Schefuß, E., Vuille, M., Novello, V.,
821 Prado, L.F., Sifeddine, A., Klein, V., Zular, A., Viana, J.C.C., Turcq, B.: Tropical South
822 Atlantic influence on Northeastern Brazil precipitation and ITCZ displacement during the
823 past 2300 years, Sci. Rep., 9, 1698, <https://doi.org/10.1038/s41598-018-38003-6>, 2019.

824 Utida, G., Cruz, F.W., Santos, R.V., Sawakuchi, A.O., Wang, H., Pessenda, L.C.R., Novello,
825 V.F., Vuille, M., Strauss, A.M., Borella, A.C., Stríkis, N.M., Guedes, C.C.F., De Andrade,
826 F.D., Zhang, H., Cheng, H., Edwards, R.L.: Climate changes in Northeastern Brazil from
827 deglacial to Meghalayan periods and related environmental impacts, Quat. Sci. Rev.,
828 250, 106655, <https://doi.org/10.1016/j.quascirev.2020.106655>, 2020.

829 Vera, C., Higgins, W., Amador, J., Ambrizzi, T., Garreaud, R., Gochis, D., Gutzler, D.,
830 Lettenmaier, D., Marengo, J., Mechoso, C.R., Nogues-Paegle, J., Silva Dias, P.L.,
831 Zhang, C.: Toward a Unified View of the American Monsoon Systems, J. Clim., 19, 4977-
832 5000, <https://doi.org/10.1175/JCLI3896.1>, 2006.

833 Vuille, M., Burns, S.J., Taylor, B.L., Cruz, F.W., Bird, B.W., Abbott, M.B., Kanner, L.C.,
834 Cheng, H., Novello, V.F.: A review of the South American monsoon history as recorded



- 835 in stable isotopic proxies over the past two millennia, *Clim. Past*, 8, 1309–1321,
836 <https://doi.org/10.5194/cp-8-1309-2012>, 2012.
- 837 Wang, X., Edwards, R.L., Auler, A.S., Cheng, H., Kong, X., Wnag, Y., Cruz, F.W., Dorale,
838 J.A., Chiang, H.-W.: Hydroclimate changes across the Amazon lowlands over the past
839 45,000 years, *Nature*, 541, 204–207, <https://doi.org/10.1038/nature20787>, 2017.
- 840 Zhang, H., Cai, Y., Tan, L., Cheng, H., Qin, S., An, Z., Edwards, R.L., Ma, L.: Large variations
841 of $\delta^{13}\text{C}$ values in stalagmites from southeastern China during historical times:
842 implications for anthropogenic deforestation, *Boreas*, 44, 511–525,
843 <https://doi.org/10.1111/bor.12112>, 2015.
- 844 Zhang, H., Cai, Y., Tan, L., Qin, S., An, Z.: Stable isotope composition alteration produced
845 by the aragonite-to-calcite transformation in speleothems and implications for
846 paleoclimate reconstructions, *Sediment. Geol.*, 309, 1–14,
847 <https://doi.org/10.1016/j.sedgeo.2014.05.007>, 2014.
- 848 Ziese, M., Rauthe-Schöch, A., Becker, A., Finger, P., Meyer-Christoffer, A., Schneider, U.:
849 GPCP Full Data Daily Version 2018 at 1.0°: Daily Land-Surface Precipitation from Rain-
850 Gauges built on GTS-based and Historic Data [dataset],
851 https://doi.org/10.5676/DWD_GPCP/FD_D_V2018_100, 2018.
- 852 Zular, A., Utida, G., Cruz, F.W., Sawakuchi, A.O., Wang, H., Bicego, M. Giannini, P.C.F.,
853 Rodrigues, S.I., Garcia, G.P.B., Vuille, M., Sifeddine, A., Zocatelli, R., Turcq, B., Mendes,
854 V.R.: The effects of mid-Holocene fluvio-eolian interplay and coastal dynamics on the
855 formation of dune-dammed lakes in NE Brazil, *Quat. Sci. Rev.*, 196, 137–153,
856 <https://doi.org/10.1016/j.quascirev.2018.07.022>, 2018.